ASEAN Engineering Journal

Full Paper

GREEN SYNTHESIS AND CHARACTERIZATION OF FE DOPED TIO_2 NANOPARTICLES USING *LAWSONIA INERMIS* LEAF AQUEOUS EXTRACTS AS REDUCTANT FOR PHOTOCATALYTIC ACTIVITY

Article history
Received
28 December 2022
Received in revised form
24 May 2023
Accepted
22 June 2023
Published online
31 August 2023

Syamsutajri Syamsol Bahri[a,b], Zawati Harun[a,b*], Wan Norhayati Wan Salleh[c], Rosniza Hussin[a,b], Nur Hanis Hayati Hairom[d], Noor Hasliza Kamaruddin[a,b], Hatijah Basri[e], Nurul Izwanie Rasli[e], Afiqah Rosman[c], Mohd Riduan Jamaluddin[f], Ainun Rahmahwati Ainuddin[b]

[a]Integrated Material Process, Advanced Materials and Manufacturing Centre, Institute Integrated Engineering, Universiti Tun Hussein Onn Malaysia, 86400 Batu Pahat, Johor, Malaysia
[b]Faculty of Mechanical and Manufacturing Engineering, Universiti Tun Hussein Onn Malaysia, 86400 Batu Pahat, Johor, Malaysia
[c]Advanced Membrane Technology Research Centre, Universiti Teknologi Malaysia, 81310 UTM Johor Bahru, Johor, Malaysia
[d]Faculty of Technology Engineering, Universiti Tun Hussein Onn Malaysia, 86400 Batu Pahat, Johor, Malaysia
[e]Faculty of Applied Sciences and Technology, Universiti Tun Hussein Onn Malaysia, 86400 Batu Pahat, Johor, Malaysia
[f]Faculty of Mechanical Engineering Technology, Universiti Malaysia Perlis, 02600 Kangar, Perlis, Malaysia

*Corresponding author
zawati@uthm.edu.my

Graphical abstract

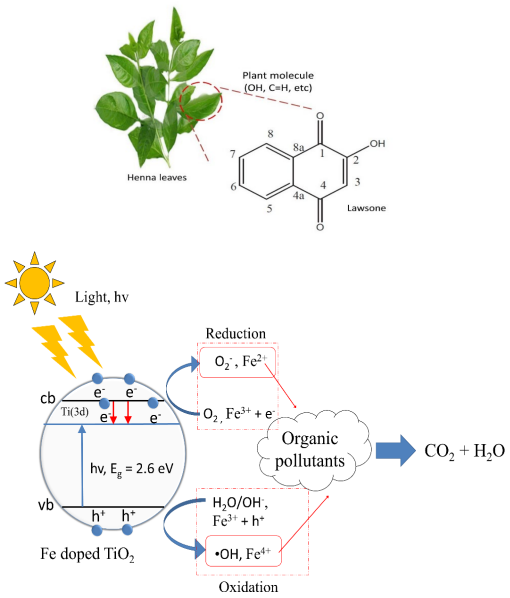

Abstract

Recently, the improvement and advancement in synthesizing nanoparticles via eco-friendly technique have been intensively explored since the used conventional physical and chemical methods always associated to the intensive energy usage and toxic waste pollution Therefore, nanoparticles synthesized from green route technique has initiate an interest among researchers due to its clean and eco-friendliness approach. In this study, the Fe doped TiO_2 were synthesized using *lawsonia inermis* aqueous leaf extracts that act as reducing agent as well as capping and stabilizing agent. The green synthesized powder was then calcined and characterized using XRD, FESEM, EDX, FTIR and UV-Vis while photocatalytic activity was evaluated based on photodegradation efficiency of methylene blue (MB). The new obtained green calcined powder was found to have a crystalline phase (anatase structure) with crystallite size, 6.79 nm identified by XRD. The FESEM test shows the average particle size of the green synthesized calcined Fe doped TiO_2 is in the range of 54.5 nm with capping agent (phyto-constituents) authorized by FTIR spectra. From EDX analysis, Fe ions was successfully incorporated into TiO_2 compound during synthesis process confirmed by the presence of Fe element. It was observed that the band gap energy for green calcined Fe doped TiO_2 is approximately 2.66 eV. The green synthesized calcined Fe doped TiO_2 sample presented the highest photocatalytic activity efficiency under uv light irradiation for 3 hour which is 92.2% with only 7.8% of MB remained, this value is slightly higher than that of commercial P25 powder which is 90.7%. In conclusion, the green synthesis technique of using *lawsonia inermis* as natural resources as reduction agent was able to produce nanoparticles Fe doped TiO_2. Moreover, the properties of Fe doped TiO_2 nanoparticles has strong potential to be used as a photocatalyst since this sustainable green synthesis technique able to produce better nanoparticles properties as compared to conventional synthesis.

Keywords: Fe doped TiO_2, green synthesis, nanoparticles, plant extract, biosynthesis

1.0 INTRODUCTION

The green synthesis has attained more attraction as it offer more environmental sustainable eco-friendly when applying and dealing with more natural materials in producing nanoparticles [1]–[3]. Besides, it is the most efficient, naturally functional, and a cost-effective method available and easily scalable for the large scale synthesis of nanoparticles production [4]–[7]. The use of non-toxic nature materials like plant extracts (leave, flower, bark, seed, and peels), fruits and other natural sources such as bacteria, fungi and enzymes that able to replace dangerous chemicals substances and reaction has widen the potential usage of these green synthesis product to various application. As reported previously, green synthesis technique able to produce materials with smaller and homogenous geometry that allow to provide larger specific surface area and demonstrate higher catalytic reactivity [8]–[12]. Furthermore, this green method is not only simple, easy and faster but also , reliable, stable and acceptable to be used as compared to other conventional methods [13]–[16]. The biological compounds that act as the capping, stabilizing and reducing agent from the natural extracts derived from different plants can make a desirable improved method for nanoparticles preparation [8]. Moreover, natural antioxidants that comes from the largest group of plant-based polyphenols are capable to be use in pharmaceutical (neutraceuticals and drugs) and food industry (food additives) because they can create a potential desirable of chemical structure from a broad range of bioactive secondary metabolites to produce nanoparticles as they can act as reducing agent in the synthesis process [17]. The plant extract offer a perfect green alternative for the nanoparticles biosynthesis because of its non-exposure to toxicity from hazardous chemicals, as compared to other natural based materials such as bacteria and algae [18]. Thus, the potentiality of preparing nanoparticles from the reaction with aqueous extract of the plant has been intensively explored and researched. The existence of most of phytobiochemical components (tannic acid, functional groups-alcohols, carboxylic acid, flavonoids, phenolics, polyphenols) that may present depending upon plant's type and plant's composition that able to enhance the reaction as well as provide better reducing, capping or stabilizing agents [19]–[21].

Meanwhile, the quality of the synthesized particles depends much on the chemical structure and composition such as nanoparticles of TiO_2, the crystallite size with certain limit of band gap effectively enhances the photocatalytic activity. In particular, for high photocatalytic activity can be achieved with smaller crystallite size, high anatase composition and broad specific surface area [22]. The approach of integration the Fe^{3+} dopants within the structure of TiO_2 photocatalyst formation able to improve and enhance photocatalytic of TiO_2 performance. As reported the integration of Fe^{3+} dopants can effectively reduce its light sensitivity and improve the TiO_2 electronic structure by reducing electron-hole recombination rate of the photogenerated charge carriers of the smaller crystals as illustrated in modified Figure 1 according to Mahy et al. [23] and Gharagozlou and Bayati [24]. By referring to Figure 1, it shows that the charge transfer process involved during photocatalysis of Fe doped TiO_2 by trapping electrons (Fe^{3+} changes to Fe^{2+}) and the holes (change to Fe^{4+}) of transition metals introduced in the bandgap. These electrons capture the excited electrons from the titania valence band, thereby suppressing/prohibiting the recombination of charge carriers. Both Fe^{2+} and Fe^{4+} species are unstable and react with adsorbed O_2 and hydroxyl to generate reactive oxygen species. Thus, result a red shift in the absorption edge and increase photocatalytic efficiency. It is also said that its semi full electronic configuration and ion radius close to Ti^{4+} increase photocatalytic efficiency [25]-[26]. A study by Teng et al. [25], has shown that the Fe incorporate in TiO_2 can broaden its effective range into the visible light range from ultraviolet range. By inserting dopants into the octahedral lattice structure of doped TiO_2, enhancing its physicochemical characteristics, thus crystallite size of TiO_2 is suppressed by inserting dopants [26]. This occurs during the dehydration process, the phase transformation of anatase to rutile can be discarded when the nucleation barrier is suppressed by thermal energy. Previous reported paper has shown that Fe is suitable for industrial applications as it is easy to prepare, low cost and consider to be one of the most suitable dopant for photocatalytic activity [27].

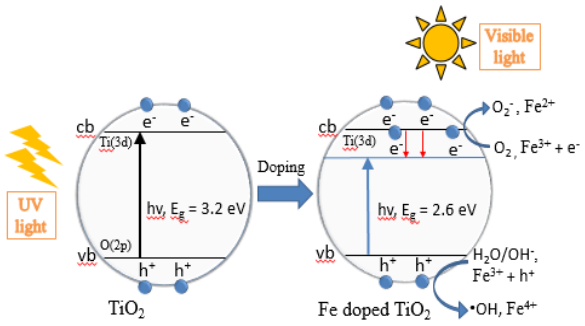

Figure 1 The process of charge transfer between excited electrons from the valence band (vb) to conduction band (cb) of TiO_2 with Fe^{3+} ions of Fe doped TiO_2

In this paper, Fe doped TiO_2 powders are synthesized using *lawsonia inermis* (henna) aqueous plant extract via green synthesis method. *Lawsonia inermis* leaves contain a variety of bioactive molecules such as lawsone. Hydroxyl and carbonyl groups may also be present in carbohydrates, flavonoids and phenolic compounds. Both hydroxyl and carbonyl groups are strong reducing agents that are responsible for the bio reduction of Fe^{3+} ions which is necessary for the synthesis process. Lawsone as shown in Figure 2 or hennotannic acid (a red-orange pigment) is the major bioactive constituent of *Lawsonia inermis* that carry hydroxyl on the quinone ring and known as the simplest naphthoquinones that occur naturally [28]. The phytochemical constituent of lawsone originated from the leaf extract known as 2-hydroxy-1, 4-napthoquionone shows significance role in the Fe doped TiO_2 nanoparticles in term of reduction and formation [29]. Lawsone has also impressive benefits such as non-hazardous, it reacts without any adverse effect to environment [30].

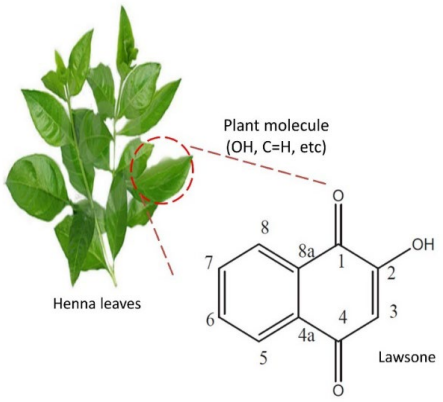

Figure 1 Lawsonia inermis with its major bioactive constituent, lawsone

Improvement of the green synthesize technique require more research investigation in terms of its production and application [31]. Thus, the present work aims to synthesize Fe doped TiO_2 nanoparticles using *lawsonia inermis* aqueous leaf extracts as reducing agent, explore the chemical interaction bonding between the organic and the metal oxide itself and to characterize the powder obtained. Advantages through understanding the interaction such as chemical bonding and functional group between plant extract with metal oxide and characteristics of the Fe doped TiO_2 nanoparticles synthesized via green synthesis methods can provide researchers with different perceptions towards characterization and photocatalysis results obtained when the Fe doped TiO_2 nanoparticles are integrated into green synthesis method. Finally, the performance of photocatalytic activities of the nanoparticles were tested and measured. The synthesis method chosen was very practical and cost-effective because only precursor used without chemicals added in comparison to chemical method thus making it as environmentally friendly and a suitable approach for gaining a sustainable synthesis of Fe doped TiO_2 nanoparticles using *lawsonia inermis* aqueous extract as reducing agent and also can be an alternative to chemical methods.

2.0 METHODOLOGY

Raw green leaf of *lawsonia inermis* were collected from local garden in Parit Raja, Batu Pahat district (Malaysia) to be used in this work. Iron (III) nitrate nonahydrate [$Fe(NO_3)_3.9H_2O$] used as Fe precursor, tetrabutyl titanate ($Ti(BuO)_4$) used as TiO_2 precursor and the methylene blue used as the target pollutants were purchased from Merck (Malaysia), Sigma–Aldrich (Germany), and Merck, India respectively. The P25 powder from Degussa (Germany) were used and regarded as commercial TiO_2. All of the received chemicals were used without any further purification. Double distilled water was used to prepare solutions throughout the experiments.

2.1 Preparation of *Lawsonia inermis* Aqeous Leaf Extracts

Firstly, the raw green leaf of *lawsonia inermis* were separated from the stems. In order to remove any adherent particles, 50g of fresh leaves were thoroughly washed and undergo drying process at ambient temperature. The leaves were mix with 500 ml distilled water, boiled at 80°C for 4-5 hours and filtered using whatman filter paper. Then, the aqueous leaf extracts were stored at 4°C in refrigerator for further use. The schematic illustration of the aqeous leaf extracts preparation of *lawsonia inermis* is illustrated as in Figure 3.

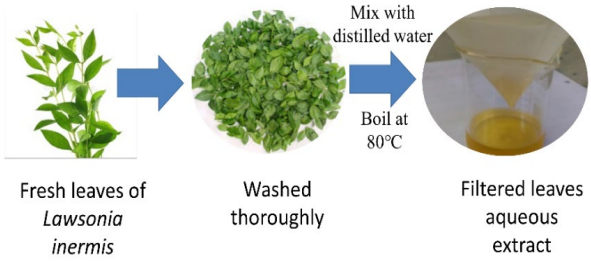

Figure 3 Schematic illustration of the aqeous leaf extracts preparation of *lawsonia inermis.*

2.2 Green Synthesis of Fe doped TiO_2 Nanoparticles

At 50 °C, 10 ml of $Ti(OBu)_4$ was added into a beaker containing 50 ml of *lawsonia inermis* aqueous leaf extract that has been filtered. They were stirred continuously using motor rotator for 60 min. Then, 1.0 g of Fe $(NO_3)_3.9H_2O$ was added under constant stirring. The mixture was dissolved completely without any additional heat treatment. The color conversion was detected after 1 h and the presence of precipitate implying the formation of Fe doped TiO_2 complex in suspension. In order to avoid any photo-induced phenomenon, the mixture was covered with aluminium foil and kept at room temperature after stirring. The mixture suspension undergoes drying process at 120 °C in an oven. In order to remove any residue of the extract, the obtained dried powder was washed thoroughly with distilled water and exposed to further heat treatment for 2 h at 90 °C. At 500 °C, the powder was calcined in a box furnace for 3 h. The schematic illustration of the green synthesis of Fe doped TiO_2 nanoparticles using aqueous leaf extract of *lawsonia inermis* is shown in Figure 4.

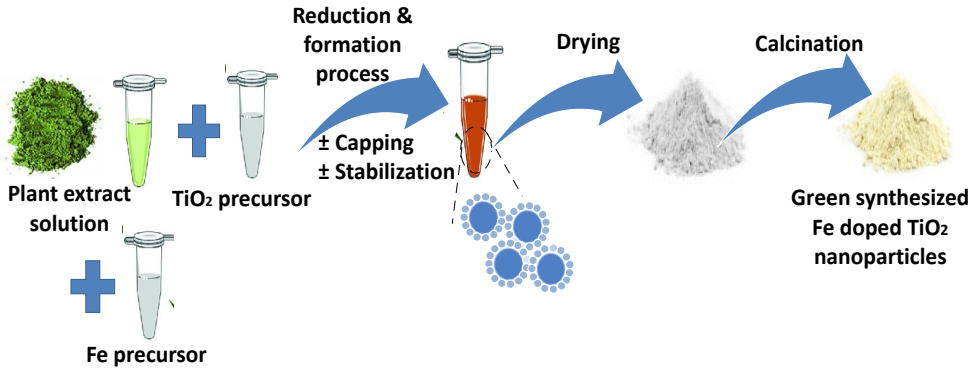

Figure 4 Schematic illustration of the green synthesis of Fe^{3+} doped TiO_2 nanoparticles using aqueous leaf extract of *lawsonia inermis*

2.3 Characterization Techniques

The obtained green synthesized Fe doped TiO_2 (FT) samples were characterized by x-ray diffraction (XRD), field emission scanning electron microscope (FESEM), energy dispersive x-ray spectroscopy (EDX), fourier transform infrared spectroscopy (FTIR) and uv-visible spectroscopy (UV-VIS). The composition of crystal phase was characterized by XRD with Cu kα radiation in the 20˚ – 90˚ range using a D8 Advanced Bruker System (2Θ as the x-ray source). The morphological structure was examined by FESEM, JSM-7600F with high resolution and EDX to verify the existence of element of the nanoparticles. Further, the capability of interaction and functional group of the plant extract and nanoparticles compressed into a thin KBr disc were identified on a FTIR, Perkin Elmer Spectrum with measurement in the ranges of 1000 to 4000 cm^{-1} in transmittance mode. The optical properties were performed by UV-VIS, UV-3600 Plus Shidmadzu, Japan with wavelength in the range of 200 to 800 nm. The estimated band gap energy values of the obtained nanoparticles were measured using the Kubelka-Munk function/Tauc plots.

The crystallite size of the samples was calculated using Debye-Scherrer equation (Eq. 1) with corrected by instrument line broadening to remove all the noise. In this equation, *D* is the crystallite size of nanoparticles, *λ* is the wavelength used (Cu Kα radiation = 1.54), *d* is the full width of the diffraction peak at half-maximum that expressed in radians which known as FWHM and *ϑ* is the Bragg angle in radians. To evaluate the change of Fe doped TiO_2 crystallinity during synthesis method, the crystallinity index of the prepared samples was calculated by using Eq. 2.

$$D = \frac{K\lambda}{d\cos\theta} \quad \text{(Eq. 1)}$$

$$\text{Crystallinity (\%)} = \frac{\sum I_{net}}{(\sum I_{total} - \sum I_{const.\ background})} \times 100 \quad \text{(Eq. 2)}$$

The percentage of crystallinity (%) can be defined by the intensity ratio of the diffraction peaks and of the sum of all measured intensity where the constant background intensity is substracted from the total intensity. The crystallinity of the prepared samples is calculated automatically by X'Pert HighScore Plus software with constant background of 83. The accuracy of this method depends much on the constant background value for samples with a high and low amorphous content. Commercial TiO_2 was used as a calibration standard with a crystallinity of 99%.

2.4 Photocatalytic Experiments

The photocatalytic activity of the green synthesized FT was performed under UV light source to observe the degradation of 10 mg/L aqueous solution methylene blue (MB) using a 30 W lamp (wavelength 312 nm). Before that, we must take into account the adsorption capability of the photocatalyst. The organic pollutant load adsorbed on the surface of nanoparticles evaluated by methylene blue degradation can influence their photocatalytic activity. In order to evaluate the photocatalytic activity efficiency, the powder loading of 0.4 g/L was magnetically stirred in the dark for 120 minutes to achieve the adsorption/desorption equilibrium before irradiated with uv light. At fixed time intervals, some amounts of the reacted solution were collected out and filtered using a syringe filter with the pore size of 0.45 µm. The absorbance of the collected filtrates was then measured at a wavelength of 660 nm to examine its maximum absorbance using a uv-vis spectroscopy at different time intervals. All the experiments were controlled at room temperature.

3.0 RESULTS AND DISCUSSION

3.1 Phase Determination

The crystal structure of the samples was determined by XRD at 2θ. The XRD spectra of the samples showed the confirmation peak of the predominantly anatase phase of TiO_2 (2θ = 25.3°; 37.8°; 48.1°; 54.4°) correspond to (011), (004), (020), (015), (121), (024), (116), (220) and (125) lattice planes are shown in Figure 5. The XRD profiles of the synthesized metal oxide nanoparticles obtained were compared with commercial synthetic TiO_2. The major detected peaks were matched with the database of ICSD file No. 98-004-5316 and observed to be the same. The noise and peak broadening in XRD patterns indicate the interference of the amorphous phase that might be due to macromolecules present in the plant extract that act as reducing agent for Fe and Ti ions [32]. Obviously, calcination

process of Fe doped TiO_2 enhanced the crystallinity of anatase phase formation with no peak of secondary phase supported by research work done by Cris et al [33] where the increased of temperature promotes crystallization , reflected in the sharper and well-defined diffraction peaks. Apart from anatase, increased temperature might formed a sharp rutile observed by Mahsyid et al [34].

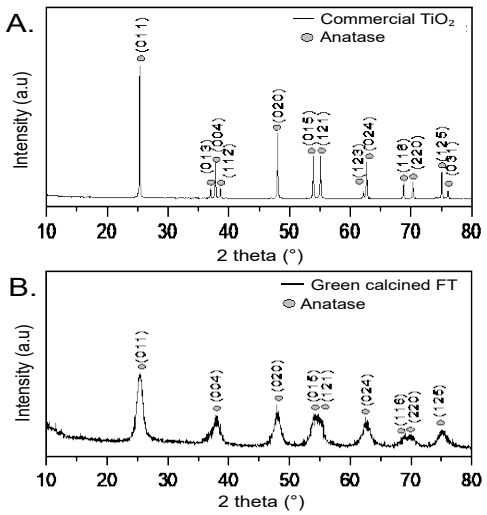

Figure 5 XRD patterns of (A) commercial TiO_2 (B) green synthesized Fe doped TiO_2.

Further observation was conducted in order to calculate the crystallite size of the samples using FWHM by referring to the highest intensity signal (2θ = 25.3˚) which corresponding to the crystallographic plane (011). Based on the formulation in (Eq 1), the crystallite size was calculated to be in the range of 73.57 nm and 6.79 nm for commercial TiO_2 and calcined Fe doped TiO_2 respectively. It was observed that the crystallite size was increased by calcinating the nanoparticles at 500˚C. At the same time, the width of the peaks decreases probably due to the rearrangement and growth of crystallite (crystallite grow faster resulting in larger size) and generation of larger clusters [22][35]. During the process, it may be suggested that smaller crystallites come closer and grow to become larger due to kinetics. So, calcination also improves the crystallinity of the nanoparticles.

A comparison of the crystal size at plane (011) with average crystallite size and the degree of crystallinity (DOC) value are listed in Table 1. Consequently, the crystallinity degree of green calcined powder would result only 59.91%. It is worth observing that the crystallinity percentage of Fe doped TiO_2 obtained is in sync with the small broad peaks of the XRD pattern depicted in Figure 5. In this study, all the deconvolution of the X-ray diffraction patterns was performed with Origin Pro 9 software considering the Gaussian function as the shape of the resolved peaks with FWHM value of 0.182 and 1.282 for synthesized samples and commercial respectively.

Table 1 Crystallite size and degree of crystallinity

Samples	Crystal size, 011 plane (nm)	Degree of Crystallinity (%)
Green calcined Fe doped TiO_2	6.79	59.91 (low)
Commercial TiO_2	73.57	99.35 (high)

We have noticed that no signal and phase formation of iron oxide was observed eventhough iron was observed and determined by EDX. The possible reason is because of the low iron loaded (1.0 g) or isomorphic substitution of Fe^{3+} ions has been effectively taken place in the anatase structure. A same pattern was obtained by a previous study mentioned that there is a very low amount of dopant in their samples and might resulted from the metal ions scattered on TiO_2 or Ti (IV) ions replaced by Fe^{3+} ions into TiO_2 matrix [36]. Moradi et al [37] suggest two possibilities of the reason why the phase was incompetent to be characterized by XRD whether the iron oxide is composed as a very thin layer on the surface of nanoparticle or organised as an amorphous phase. However, it is possible to find the amorphous iron oxide obtained from the powder synthesis and obviously cannot be discard even at small concentration. Finding from other researchers has reported that the broadening and the intensity decrease of XRD peaks are related with iron (Fe^{3+}) incorporation in the anatase (TiO_2) structure [37][25]. Consequently, a crystallization of solids may face difficulties when this incorporation occur because it may lead to variation of lattice energy of the equivalent anatase [38]. Schematic diagram illustrated in Figure 6 shows a possible overview interaction of synthesized Fe doped TiO_2 nanoparticles obtained using the green synthesis method. The plant extracts act as reductants, facilitating the formation of Fe-TiO_2 complexes, which are subsequently converted into Fe doped TiO_2 nanoparticles and favouring anatase formation.

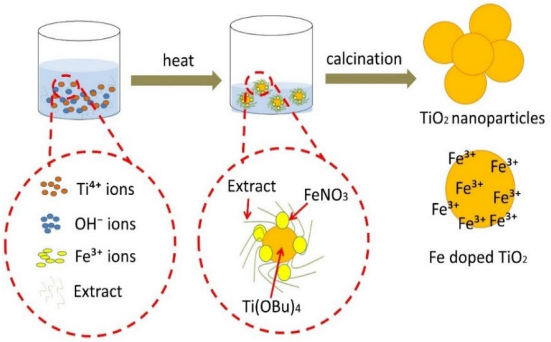

Figure 6 Schematic green synthesis diagram of Fe doped TiO_2 nanoparticles

3.2 Morphology and Element Composition

The FESEM and EDX spectroscopy were taken for the characterization of the morphology and elemental composition of the synthesized Fe doped TiO_2 powders and commercial TiO_2 respectively. FESEM images were taken at x50,000 magnifications to provide information on the physical morphology and particle size of Fe doped TiO_2 nanoparticles. As can be seen from the FESEM morphological images in Figure 7(A)(i) and (ii), the observed nanoparticles are nearly spherical structure with agglomerated to some extent. The agglomeration of smaller nanoparticles easily occurs due to the fact that the mixing composition involved in this study are originated from biological plant extract [5]. The strong hydrophobic property that exhibit by most of plant component that involve in reduction process coated onto Fe doped TiO_2 nanoparticles will has strong tendency to attach each other due to strong hydrophobic property [39]. The green synthesized

TiO_2 nanoparticles depicted in Figure 7(A)(ii) are quite polydisperse, poorly dispersed and they were agglomerated with a particle size ranging from 36–103 nm. The average particle size of the synthesized Fe doped TiO_2 nanoparticles was estimated to be 57 nm. The compounds such as phenolic, aromatic and carboxylic acid that present in the *lawsonia inermis* plant extract mainly effect on reduction and formation of the nanoparticles size as they act as a reducing agent as well as capping agent and stabilizing agent in the synthesis process [40]–[43]

The calculated crystallite size of Fe doped TiO_2 obtained in XRD in Table 1 is smaller than the average particles size shown by FESEM observation in Figure 7(A)(ii). This could be attributed by the fact that each particle consists of large, agglomerated particles that cannot be easily differentiate from single particles under microscopic observation. It also shows that the nanoparticles have a small size of crystallite by referring to the broaden diffraction peaks as reported in [44]. The same result obtained by referring to the previous related works done by [45] where all the powders obtained are more finer and consist of agglomerated particles with spherical in shape. Moreover, the powders micrographs show that the degree of agglomeration increased with further increased of Fe doping into TiO_2. Generally, particle size may be present as a single crystal, or an agglomeration of several crystals determined by FESEM/SEM. Hence, the particle size could equivalent to the sum of crystallite size of Fe doped TiO_2 [46]-[47]. In addition, the particle size of synthetic TiO_2 determined by FESEM in this work was found to be similar to the value reported in the previous work done by [47]. A reduced particle sizes may have an advantage in the chemical reactivity of powder as reported by Torres-Luna et al. [38].

The energy dispersive X-ray analysis (EDX) present with multiple peaks in the range of 0.5 keV to 5.5 keV shows that the pattern is directly related to Fe doped TiO_2 nanoparticles by referring to the vigorous peak of Fe and Ti observed in the range of 2.8-3.4 keV respectively as shown in Figure 7(B)(i) and (ii). From EDX testing, the atom's percentage and chemical composition present in the sample was analysed. Table 2 presents the percentage of O, Ti and Fe elements confirming the formation of Fe doped TiO_2 via green synthesis route. Fe ion was successfully incorporated into TiO_2 compound during synthesis process confirmed by the presence of Fe element in the analysed samples. The same results was obtained by [48] where it shows evident that the dopant metals are scattered on the TiO_2 surface.

Table 2 EDX elemental analysis of synthesized Fe doped TiO_2 and commercial TiO_2

Samples	Element	Weight (%)	Atomic (%)
Green calcined Fe doped TiO_2	O	50.74	75.90
	Ti	42.11	21.04
	Fe	7.16	3.07
	Total	100.00	100.00
Commercial TiO_2	O	51.72	76.23
	Ti	48.28	23.77
	Total	100.00	100.00

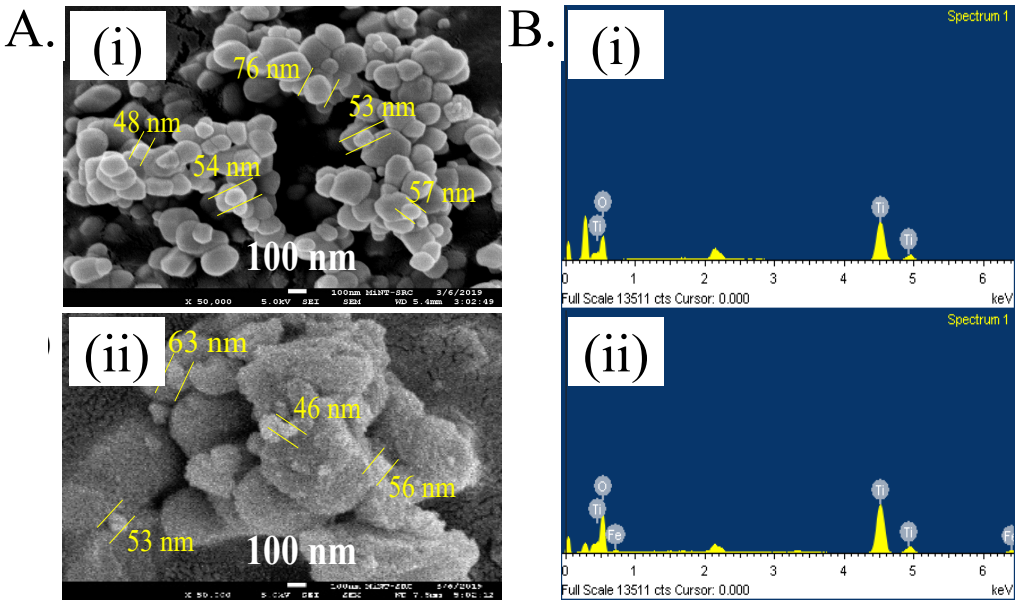

Figure 7 (A) FESEM image sample of i) commercial TiO_2 ii) calcined Fe doped TiO_2. (B) EDX image sample analysis of i) commercial TiO_2 ii) calcined Fe doped TiO_2

3.3 Functional Group

Fourier transform infrared (FTIR) spectra analysis was performed to determine the functional groups of the phytobiochemical present in the synthesized sample which give significant role as reduction and stabilizing agent in the synthesis process. This IR spectrum reading includes the stretching or vibration bands of the phytobiochemical compounds [49].The spectra of *lawsonia inermis* aqueous leaf extract, *lawsenia inermis* dry powder, commercial TiO_2 and

infrared (IR) spectrum of synthesized Fe doped TiO_2 nanoparticles were shown in Figure 8(A) and (B). Results in Figure 8(A) indicated that the dry leaf powder presented higher phytobiochemical compound contents than the aqueous leaf extract. Both spectrum reveals two major absorption band namely hydroxyl (O-H) and carbonyl (C=O) functional group present in the plant extract which acts as stabilizing and capping agent. The absorption band at 3370 cm^{-1} and 2960 cm^{-1} indicate the free hydroxyl groups correspond to the O-H bond stretching and denotes the aqueous phase which participated in the synthesis reaction. The stretching of carbonyl groups (C=O) in lawsone was observed by peak at 1625 cm^{-1} for both aqueous extract and dry leaf powder. The FTIR spectrum of dry powder of *lawsonia inermis* showed characteristic bands at 1124 cm^{-1} and 1430 cm^{-1} suggesting the existence of C-O stretching carboxylic acids that could not be detected in aqueous leaf extract [5]. The bands appeared in Fe doped TiO_2 nanoparticles spectrum but the position shifted to 1120 cm^{-1} and 1460 cm^{-1} which gives the evidence for conjugation and presence of flavonoids on the surface of nanoparticles [50].

In green synthesized Fe doped TiO_2, the band shifts from 3300 cm^{-1} to a large broad peak at around 3100-3400 cm^{-1}, which appear due to the phytobiochemical compounds of O-H stretching associated with lawsone and tannin since *Lawsonia inermis* contain a variety of constituents such as lawsone, flavonoids, gallic acid and tannin thus having different functional groups [43], [50] and [51]. The broad absorption peaks can also be appointed to absorption of surface O-H bonds (stretching modes) and might be associated with O–H vibration of the adsorbed water (H_2O molecules) [45], demonstrating that much more H_2O adsorbed on the surface of nanoparticles, which capable to produce much more -OH radicals after light irradiation. This bending vibration of adsorbed water also might be due to initiation of Fe (III) ions into the nanoparticles matrix that increased the absorption of more loading of OH groups. This hydrophilic property will contribute to intramolecular hydrogen bonding between the OH group and adjacent oxygen group. Thus, this will create Ti-OH stretching vibration bond presence in the spectrum that could not be eliminate simply without heating at relatively high temperature at 500˚C. If we go through the FTIR spectrum of aqueous leaf extract, we find that the absorption bands are shifted from 1625 cm^{-1} to around 1650 cm^{-1} in the synthesized spectrum. This shifting of peak position proves the interaction of phytobiochemicals in plant extract with nanoparticles or specifically means that the C=O group contribute a significant role in this formation [52]. The extract may adhere to the nanoparticles surface by various forces such as hydrophobic interaction, chemisorption and/or electrostatic attraction therefore forming a stable nanoparticle.

Remarkably, the surface-adsorbed water and phenolic hydroxyl groups slightly decreased with temperature increased. From previous study, the enhancement of the photocatalytic activity was obtained when the hydroxyl groups on the surface of samples interact with photogenerated holes which can contribute to good charge transfer and inhibits the electron-hole pairs recombination [53]. These positive charge transfers from hydroxyl groups can accelerate the adsorption and degradation of organic pollutants. The intensity of Fe doped TiO_2 nanoparticles peaks synthesized by leaf extract decreased might be due to the physio-absorption process interaction between nanoparticles and plant extract and this proved that the reduction/capping process was occurred during the synthesis. The active compound in the extract itself, for example lawsone might be the one that acts as reducing agent of Fe doped TiO_2. The correlation between FTIR spectra with qualitative phytobiochemical screening of *lawsonia inermis* plant extract offers an insight and could enhance understanding in terms of nanoparticles surface interaction.

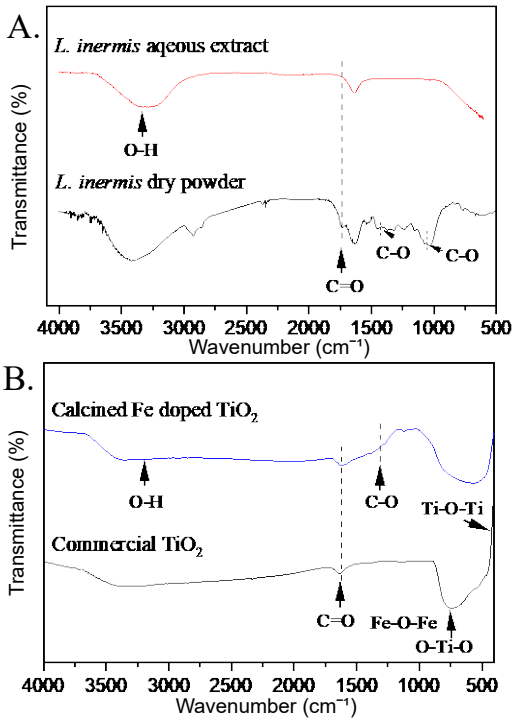

Figure 8 FTIR spectra of (A) *lawsonia inermis* aqeous leaf extract and dry powder (B) synthesized Fe doped TiO_2 and commercial TiO_2

All the synthesized nanoparticles have strong intensity of metal oxide bond. The bond is well depicted in Figure 8 by the wavelength in the range of 400-1000 cm^{-1} that associated to stretching vibration of Ti-O and Ti-O-Ti bonding as well as O-Ti-O vibration and the symmetric Fe-O-Fe stretching vibration. [54] and [55]. The FTIR analysis affirmed that Fe doped TiO_2 nanoparticles synthesized by green method via *lawsonia inermis* aqeuos leaf extract are functionalized with phenolic, aromatic and carboxylic acid. These compounds could prompt the reduction process and provide stability to the nanoparticles. This qualitative phytochemical screening of the aqueous leaves extracts and dry leaves of *lawsonia inermis* when correlated with FTIR spectra offers an insight and could result in better understanding of its interaction with nanoparticles surface.

3.4 Optical Measurement

The UV-visible diffusion absorption spectra and $(K.M.E)^2$ versus photo energy (hv) has been plotted in wavelength range of 200 - 800 nm to present the variation of the optical absorbance between nanoparticles with commercial TiO_2 for comparison in Figure 9(A) and (B). Noted that the maximum absorbance observed in the graph plot is the feature peak of surface plasmon resonance (SPR) formed by the resonant conduction

electrons in metallic nanoparticles stimulated by incident light as reported by Rasheed et al. [56] and Liao et al. [57].

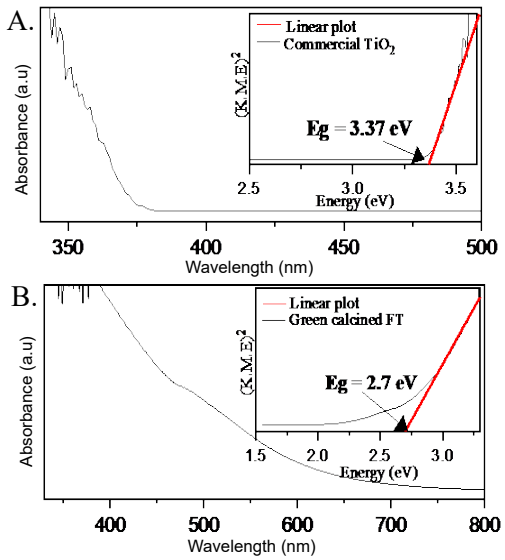

Figure 9 Tauc plot of (A) commercial TiO_2 and (B) green synthesized Fe doped TiO_2

Notably, the absorption edge for nanoparticles clearly show the shift of the wavelength towards visible region (near 650 nm) [58]. It was observed that the band gap energy for commercial TiO_2 and green calcined Fe doped TiO_2 are approximately 3.37 and 2.66 eV respectively. These optical band gap transition energies were estimated from the intercepts of linear portion of the Kubelka-Munk function $(K.M.E)^2$ versus photon energy (hv) where a good approximation will be obtained from the tangent line interception to the plot. It is found that the green synthesis nanoparticles have a lower band gap than the commercial nanoparticles.

3.5 Photocatalytic Activity

The impact of Fe^{3+} ions on titania's catalytic activity has always been an interesting study. Therefore, a number of degradation tests of methylene blue (MB) under UV light irradiation by using green synthesized Fe doped TiO_2 photocatalyst were carried out. The adsorption of methylene blue (MB) dye on the Fe doped TiO_2 nanoparticles was monitored by measuring the absorbance values at different time intervals as illustrated in the Figure 10(B). This adsorption difference might be associated to the electrostatic forces by both MB dye and the nanoparticles surface [59].

Meanwhile, MB dye was irradiated with UV light in the absence of the nanoparticles as a control experiment. The absorption peak feature of methylene blue at 660 nm was used to monitor the photocatalytic degradation process with uv light exposure at different time intervals. There was no major change in the MB dye concentration observed in the findings. A slight decrease in absorbance was detected where the pollution concentration reduces to about 1.9% due to photodegradation process as illustrated in Figure 10(C). This finding also showed that the direct photolysis of MB dye was insignificant indicated by the absence of the nanoparticles. The percent of degradation the nanoparticles in the aqueous solution was calculated in Eq. 4 as below:

$$\text{Degradation (\%)} = \frac{C_o - C_t}{C_o} x\ 100 \quad \text{(Eq.4)}$$

where Co is the initial concentration at time t = 0, and C_t is the concentration time interval. It can be seen that green calcined Fe doped TiO_2 sample presented the highest photocatalytic activity efficiency under uv light irradiation for about 3 hour with only 7.8% of MB remained, this value is slightly higher than that of P25 which is 90.7%. In Figure 10(A), the standard curve of MB indicate that the concentration of MB and absorbance form a good linear relationship with correlation coefficient R = 0.99505 and the fitting standard curve equation is: A = 0.00758 + 0.02843x.

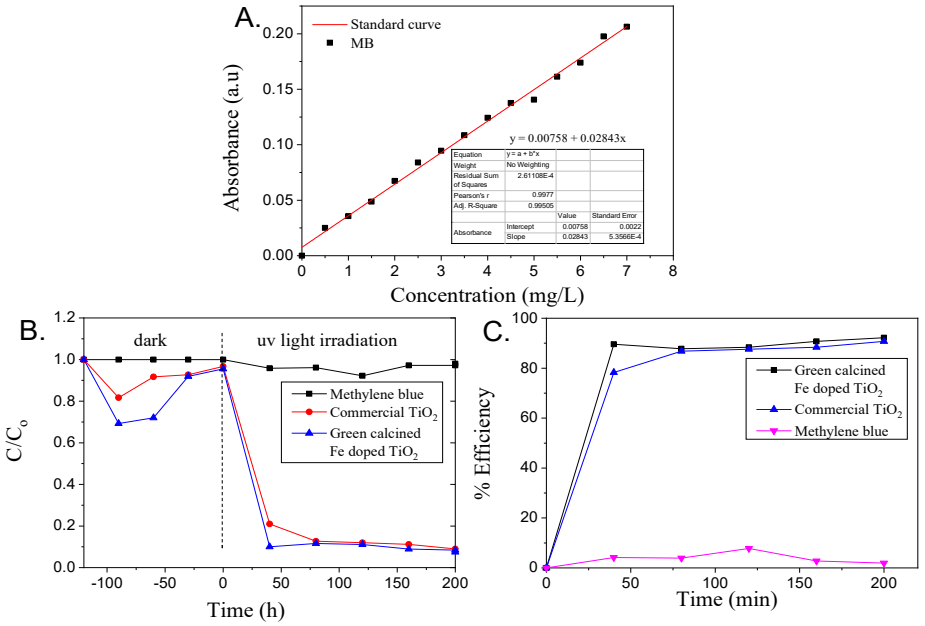

Figure 10 (A) Standard calibration curve of methylene blue. (B) The photocatalytic activity of synthesized green Fe doped TiO_2 and commercial TiO_2 under uv light irradiation and without light. (C) Photodegradation efficiency of synthesized green Fe doped TiO_2 and commercial TiO_2.

As we are well informed that there are various types of photocatalyst available in the market due to tremendous advancement in the field of photocatalysis thus the efficiency of such photocatalysts is become important and need to further research. In this study, we compared the photodegradation result between the green synthesized powders with commercial photocatalyst. It shows that the green synthesized Fe doped TiO_2 calcined at 500˚C sample exhibited a higher efficiency compared to the commercial sample in degrading the MB pollutant in uv light with a difference of 1.5% points.

The proposed schematic mechanism diagram of photocatalytic reaction occurs on the Fe doped TiO_2 surface has been represented in Figure 11 based on previous reported by Sood et al. [36] Azeez et al. [59] . In the reported work, photogenerated electrons and holes are generated when uv light exposed to the surface of nanoparticles (Eq. 6). The Fe^{3+} ions that are present in the surface of TiO_2 can act as electron and hole trap (Eq. 7-8) thus generate the less stable Fe^{2+} and Fe^{4+} ions (due to half-filled stable d5 configuration) compared to Fe^{3+}. As a result, the trapped charges can be easily released to create stable Fe^{3+} ions and lead to generation of $OH^{\bullet}$ radical and O_2^- anion (Eq. 9-11). However, they may act as recombination centers for the charge carriers if Fe concentration is high, thereby reducing the photocatalytic activity (Eq. 12-13). There is a possibility to generate a number of high redox potentials of charged species and radicals through a redox reaction's series (Eq. 14-17). Thus, the intermediates (S) formed when the organic pollutant molecules (P) are oxidized by these highly oxidizing species thus obtaining a complete mineralization (Eq. 18). The general photocatalysis degradation of the organic pollutant mechanism has been schematically shown from (Eq. 6–18).

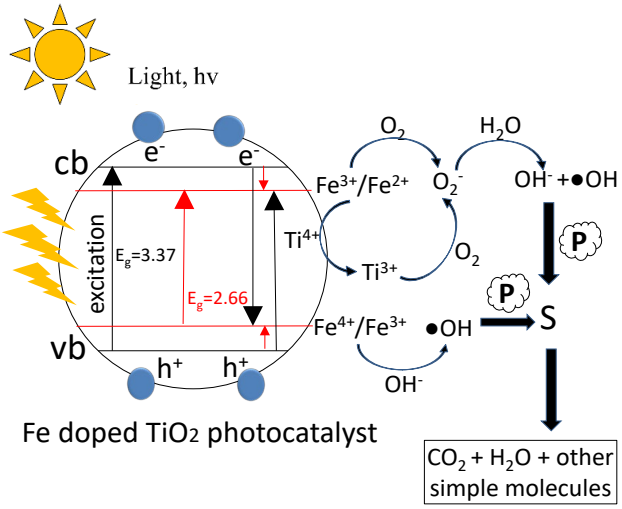

Figure 11 The proposed schematic mechanism diagram of photocatalytic reaction occurs on the Fe. doped TiO_2 surface

1. Absorption of efficient photons:

$$Fe^{3+}doped\ TiO_2 + hv \rightarrow e_{CB}^- + h_{VB}^+ \qquad (6)$$

2. Generation of potential charged species and radicals through a series of redox reactions:

$$Fe^{3+} + e^- \rightarrow Fe^{2+} (7)$$

$$Fe^{3+} + h^+ \rightarrow Fe^{4+} (8)$$

$$Fe^{2+} + O_2 \rightarrow Fe^{3+} + O_2^- (9)$$

$$Fe^{2+} + Ti^{4+} \rightarrow Fe^{3+} + Ti^{3+} \quad (10)$$

$$Fe^{4+} + OH^{-} \rightarrow Fe^{3+} + OH^{\bullet} \quad (11)$$

$$Fe^{3+} + e^{-} \rightarrow Fe^{2+} \quad (12)$$

$$Fe^{2+} + h^{+} \rightarrow Fe^{3+} \quad (13)$$

$$Ti^{3+} + O_2 \rightarrow Ti^{4+} + O_2^{-} \quad (14)$$

$$O_2^{-} + h^{+} \rightarrow O^{-} \quad (15)$$

$$O^{-} + h^{+} \rightarrow O^{\bullet} \quad (16)$$

$$O^{-} + H_2O \rightarrow OH^{\bullet} + OH^{-} \quad (17)$$

3. Complete mineralization

$$Pollutant + OH^{\bullet} \rightarrow intermediates + OH^{\bullet}/OH^{-}/O_2^{-} \rightarrow CO_2 + H_2O/other\ simpler\ molecules \quad (18)$$

4.0 CONCLUSION

In conclusion, the synthesis of Fe doped TiO_2 nanoparticles using a green approach has proven to be successful. The presence of the active phytochemical and biocompounds in the *lawsonia inermis* aqueous leaf extract during the synthesis process plays a crucial role as reducing agent. The characterization of the synthesized sample through XRD, UV-vis and FESEM analysis has shown that the synthesized sample has anatase phase structure, with band gap 2.66 eV and average particle size in the average range of 54.5 nm, respectively. Moreover, the presence of Fe element in the synthesized sample shown by EDX analysis provides proof that Fe ions were successfully incorporated into the TiO_2 compound throughout the synthesis process. With the obtained data, this method has advantage for Fe doped TiO_2 nanoparticles production as it is environmental friendly, and can operate at minimal temperature, resulting in a faster reaction. This contrasts with the conventional TiO_2 synthesis method, which frequently uses hazardous chemical and high temperature, as demonstrated in numerous examples from the literature. Furthermore, this finding highlights the potential of these nanoparticles for applications that require efficient photocatalysis. The green synthesized Fe doped TiO_2 nanoparticles exhibit a significant improvement in photocatalytic activity for the degradation of methylene blue as it exhibited the highest photocatalytic activity efficiency with 92.2% of the MB dye degraded compared to commercial TiO_2. In summary, the synthesis of Fe doped TiO_2 nanoparticles using *lawsonia inermis* leaf extracts represents a promising and environmentally friendly approach. The nanoparticles exhibit enhanced photocatalytic activity and can be utilized in various fields where efficient degradation of organic pollutants is desired.

Acknowledgement

This research was supported by Ministry of Higher Education Malaysia (MOHE) through the Fundamental Research Grant Scheme (FRGS/1/2020/TK0/UTHM/02/45) and partially sponsored by Universiti Tun Husssein Onn Malaysia (UTHM). The authors also would like to thank to Universiti Teknologi Malaysia (UTM) for sponsoring this work under HICOE AMTEC (A.J090301.5300.07092).

References

[1] M. N. Gallucci *et al.* 2017. Silver nanoparticles from leafy green extract of Belgian endive (Cichorium intybus L. var. sativus): Biosynthesis , characterization, and antibacterial activity. *Materials Letter.* 97: 98–101. DOI: https://doi.org/10.1016/j.matlet.2017.03.141

[2] L. Wang, J. Xie, T. Huang, Y. Ma, and Z. Wu. 2017. Characterization of silver nanoparticles biosynthesized using crude polysaccharides of Psidium guajava L. leaf and their bioactivities. *Materials. Letter.* 208: 126–129, 2017. DOI : https://doi.org/10.1016/j.matlet.2017.05.014

[3] N. Senthilkumar, E. Nandhakumar, P. Priya, D. Soni, M. Vimalan, and I. Vetha Potheher. 2017. Synthesis of ZnO nanoparticles using leaf extract of: Tectona grandis (L.) and their anti-bacterial, anti-arthritic, anti-oxidant and in vitro cytotoxicity activities. *New Journal of Chemical*. 41(18): 10347–10356. DOI: https://doi.org/10.1039/c7nj02664a

[4] G. V Khade, M. B. Suwarnkar, N. L. Gavade, and K. M. Garadkar. 2015. Green synthesis of TiO_2 and its photocatalytic activity. *Journal of Materials Science: Materials in Electronics*. 26: 3309–3315. DOI: https://doi.org/10.1007/s10854-015-2832-7

[5] R. Dobrucka and J. Długaszewska. 2016. Biosynthesis and antibacterial activity of ZnO nanoparticles using Trifolium pratense flower extract. *Saudi Journal of Biological Sciences.* 23(4): 517–523. DOI : https://doi: 10.1016/j.sjbs.2015.05.016

[6] S. Ganesan *et al.* 2016. Green engineering of titanium dioxide nanoparticles using Ageratina altissima (L.) King & H.E. Robines. medicinal plant aqueous leaf extracts for enhanced photocatalytic activity. *Annals of Phytomedicine: An International Journal.* 5(2): 69–75. DOI : 10.21276/ap.2016.5.2.8.

[7] M. K. Husam. 2018. The effect of pH , temperature on the green synthesis and biochemical activities of silver nanoparticles from Lawsonia inermis extract. *Journal of Pharmaceutical Sciences and Research*. 10(8): 2022–2026.

[8] E. K. Baghkheirati *et al.* 2015. Modelling and optimization of Ag-nanoparticle biosynthesis mediated by walnut green husk extract using response surface methodology. *Materials Letter.* 4: 4–7. DOI: 10.4172/2169-0022.1000164

[9] M. Sathishkumar, N. P. Subiraminiyam, and M. Sasikumar. 2017. *Antibacterial activities of Zinc Sulphide nanoparticles using leaf extract of Lawsonia inermis*. Nehrucolleges.Net. Retrieved January, 10, 2019 from http://www.nehrucolleges.net/images/pdf/2017/Antibacterial-activities-ECS.pdf

[10] M. Sundrarajan, S. Jegatheeswaran, S. Selvam, R. Gowri, M. Balaji, and K. Bharathi. 2017. Green approach : Ionic liquid assisted synthesis of nanocrystalline ZnO in phyto medium and their antibacterial investigation. *Materials Letter.* 201: 31–34. DOI: 10.1016/j.matlet.2017.04.088

[11] N. Jayarambabu, K. V. Rao, and V. Rajendar. 2018. Biogenic synthesis, characterization, acute oral toxicity studies of synthesized Ag and ZnO nanoparticles using aqueous extract of Lawsonia inermis. *Materials Letter.* 211: 43–47. DOI: https://doi.org/10.1016/j.matlet.2017.09.082

[12] V. Mishra, R. Sharma, N. D. Jasuja, and D. K. Gupta. 2014. International Journal of Green and A Review on green synthesis of nanoparticles and evaluation of antimicrobial activity. *International Journal of Green and Herbal Chemistry*. 3(1): 81–94.

[13] Z. Zang, X. Zeng, J. Du, M. Wang, and X. Tang. 2016. Femtosecond laser direct writing of microholes on roughened ZnO for output

power enhancement of InGaN light-emitting diodes. *Optic Letters.* 41(15): 3463.

[14] C. Li, C. Han, Y. Zhang, Z. Zang, M. Wang, and X. Tang. 2017. Enhanced photoresponse of self-powered perovskite photodetector based on ZnO nanoparticles decorated $CsPbBr_3$ films. *Solar Energy Materials and Solar Cells*. 172: 341–346. DOI: https://doi.org/10.1016/j.solmat.2017.08.014.

[15] V. Ravichandran, S. Vasanthi, S. Shalini, S. Adnan, and A. Shah. 2016. Green synthesis of silver nanoparticles using Atrocarpus altilis leaf extract and the study of their antimicrobial and antioxidant activity. *Materials Letter*. 180: 264–267. DOI: https://doi.org/10.1016/j.matlet.2016.05.172.

[16] G. . Rao, A. CH, V. . Rao, S. C. Chakra, and P. Tambur. 2015. Green Synthesis of TiO_2 Nanoparticles using aloe vera extract. *International Journal of Advanced Ressearch in Physical Science.* 2: 28–34. DOI: https://doi.org/10.1002/yd.305

[17] T. Rasheed, M. Bilal, H. M. N. Iqbal, and C. Li. 2017. Green biosynthesis of silver nanoparticles using leaves extract of Artemisia vulgaris and their potential biomedical applications. *Colloids Surfaces B: Biointerfaces*. 158: 408–415. DOI: https://doi.org/10.1016/j.colsurfb.2017.07.020

[18] M. N. Nadagouda, G. Hoag, J. Collins, and R. S. Varma. 2009. Green synthesis of Au nanostructures at room temperature using biodegradable plant surfactants. *American Chemical Society*. 9(11): 4979–4983. DOI: https://doi.org/10.1021/cg9007685

[19] S. A. Dahoumane, C. Jeffryes, M. Mechouet, and S. N. Agathos. 2017. Biosynthesis of inorganic nanoparticles: a rresh Look at the control of shape, size and composition. *Bioengineering*. 4(14): 1–16. doi: https://doi.org/10.3390/bioengineering4010014

[20] M. Herlekar, S. Barve, and R. Kumar. 2014. Plant-mediated green synthesis of iron Nanoparticles. *Journals of Nanoparticles*. 2014: 1–9. DOI: https://doi.org/10.1155/2014/140614

[21] S. Saif, A. Tahir, and Y. Chen. 2016. Green synthesis of iron nanoparticles and their environmental applications and implications. *Nanomaterials*. 6(11): 209. DOI: https://doi.org/10.3390/nano6110209

[22] S. Phromma, T. Wutikhun, P. Kasamechonchung, and T. Eksangsri. 2020. Effect of calcination temperature on photocatalytic activity of synthesized TiO_2 nanoparticles via wet ball milling sol-gel method. *Applied Sciences*. 10(3): 993. DOI: https://doi.org/10.3390/app10030993

[23] J. G. Mahy *et al.* 2016. Towards a large scale aqueous sol-gel synthesis of doped TiO_2 : study of various metallic dopings for the photocatalytic degradation of p-nitrophenol. *Journal of Photochemistry and Photobiology A: Chemistry*. 329: 189–202. DOI: https://doi.org/10.1016/j.jphotochem.2016.06.029.

[24] M. Gharagozlou and R. Bayati. 2015. Photocatalytic characteristics of single phase Fe-doped anatase TiO_2 nanoparticles sensitized with vitamin B12. *Materials Research Bulletin*. 61: 340–347. DOI: https://doi.org/10.1016/j.materresbull.2014.10.043.

[25] H. Teng, S. Xu, D. Sun, and Y. Zhang. 2013. Preparation of Fe-doped TiO_2 nanotubes and their photocatalytic activities under visible light. *International Journal of Photoenergy*. 2013: 1-7. DOI: https://doi.org/10.1155/2013/981753.

[26] M. R. D. Khaki, M. S. Shafeeyan, A. A. A. Raman, and W. M. A. W. Daud. 2017. Application of doped photocatalysts for organic pollutant degradation - a review. *Journal of Environmental Management.* 198: 78–94. DOI: https://doi.org/10.1016/j.jenvman.2017.04.099.

[27] M. Crisan *et al.* 2015. Sol–gel iron-doped TiO_2 nanopowders with photocatalytic activity. *Applied Catalysis: A General.* 504: 130–142. DOI: http://dx.doi.org/10.1016/j.apcata.2014.10.031

[28] A. K. Jordão, M. D. Vargas, A. C. Pinto, F. D. C. Da Silva, and V. F. Ferreira. 2015. Lawsone in organic synthesis. *Royal Science of Chemistry Advances.* 5(83): 67909–67943. DOI: https://doi.org/10.1039/c5ra12785h.

[29] SCCS (Scientific Committee on Consumer Safety). Opinion on *Lawsonia inermis* (Henna). September, 19, 2013. DOI : https://doi.org/10.2772/71314.

[30] M. A. R. Bhuiyan, A. Islam, A. Ali, and M. N. Islam. 2017. Color and chemical constitution of natural dye henna (Lawsonia inermis L) and its application in the coloration of textiles. *Journal of Cleaner Production.* 167: 14–22. DOI: https://doi.org/10.1016/j.jclepro.2017.08.142.

[31] A. Nordmeier, J. Woolford, L. Celeste, and D. Chidambaram. 2017. Sustainable batch production of biosynthesized nanoparticles. *Materials Letter.* 191: 53–56. DOI: https://doi.org/10.1016/j.matlet.2017.01.032.

[32] P. S. M. Kumar, A. P. Francis, and T. Devasena. 2014. Biosynthesized and chemically synthesized titania nanoparticles : comparative analysis of antibacterial activity. *Journal of Environmental Nanotechnoly.* 3(3): 73–81. DOI: https://doi.org/10.13074/jent.2014.09.143098.

[33] M. Cris, D. Cris, A. Ianculescu, I. Nit, B. Vasile, and C. Stan. 2015. Sol–gel iron-doped TiO_2 nanopowders with photocatalytic activity. *Applied Catalysis A: General.* 504: 130–142.DOI: http://dx.doi.org/10.1016/j.apcata.2014.10.031[34]S. Mahshid, M. Askari, and M. S. Ghamsari. 2007. Synthesis of TiO_2 nanoparticles by hydrolysis and peptization of titanium isopropoxide solution. *Journal of Materials Proessing Technology.* 189: 296–300. DOI: https://doi.org/10.1016/j.jmatprotec.2007.01.040.

[35] A. Gaber, M. A. A.- Rahim, and M. N. Abdel-salam. 2014. Influence of calcination temperature on the structure and porosity of nanocrystalline SnO_2 synthesized by a conventional precipitation method. *International Journal of Electrochemical Science.* 9: 81–95. DOI: https://doi.org/10.1016/S1452-3981(23)07699-X

[36] S. Sood, A. Umar, S. K. Mehta, and S. K. Kansal. 2015. Highly effective Fe-doped TiO_2 nanoparticles photocatalysts for visible-light driven photocatalytic degradation of toxic organic compounds. *Journal of Colloid and Interface Science*. 450: 213–223. DO : https://doi.org/10.1016/j.jcis.2015.03.018.

[37] V. Moradi, M. B. G. Jun, A. Blackburn, and R. A. Herring. 2018. Significant improvement in visible light photocatalytic activity of Fe doped TiO_2 using an acid treatment process. *Applied Surface Science*. 427: 791–799.DOI : https://doi.org/10.1016/j.apsusc.2017.09.017.

[38] J. A. Torres-Luna, N. R. Sanabria, and J. G. Carriazo. 2016. Powders of iron(III)-doped titanium dioxide obtained by direct way from a natural ilmenite. *Powder Technology.* 302: 254–260.nDOI : https://doi.org/10.1016/j.powtec.2016.08.056.

[39] K. G. Rao, C. Ashok, K. V. Rao, C. Shilpa Chakra, and V. Rajendar. 2015. Synthesis of TiO_2 nanoparticles from orange fruit waste. *International. Journal of Multidiscipline Advanced Research Trends*. 2(1): 82–90.

[40] M. K. Husam. 2018. The effect of pH , temperature on the green synthesis and biochemical activities of silver nanoparticles from Lawsonia inermis extract. *Journal of Pharmaceutical Scences and Research*. 10(1): 2022–2026.

[41] M.M.S, Sherifa, *et al.* 2015. The Importance of the chemical composition of henna tree Leaves (Lawsonia inermis) and its ability to eliminate tinea pedis , with reference to the extent of usage and storage in the Saudi Society, Taif, KSA. *Journal of Pharmacy and Biological Sciences*. 10(4): 23–29. DOI: https://doi.org/10.9790/3008-10442329.

[42] S. C. G. K. Daniel, N. Mahalakshmi, J. Sandhiya, K. Nehru, and M. Sivakumar. 2013. Rapid synthesis of Ag nanoparticles using henna extract for the fabrication of photoabsorption enhanced dye sensitized solar cell (PE- DSSC). *Advanced Materials Research*. 678: 349–360. DOI: https://doi.org/10.4028/www.scientific.net/AMR.678.349.

[43] A. Gupta, S. R. Bonde, S. Gaikwad, A. Ingle, A. K. Gade, and M. Rai. 2014. Lawsonia inermis-mediated synthesis of silver nanoparticles: activity against human pathogenic fungi and bacteria with special reference to formulation of an antimicrobial nanogel. *IET Nanobiotechnology*. 8(3): 172–178. DOI: https://doi.org/10.1049/iet-nbt.2013.0015.

[44] I. Uddin, K. Ahmad, A. A. Khan, and M. A. Kazmi. 2017. Synthesis of silver nanoparticles using Matricaria recutita (Babunah) plant extract and its study as mercury ions sensor. *Sensing Bio-Sensing Research.* 16(2017): 62–67.nDOI : https://doi.org/10.1016/j.sbsr.2017.11.005.

[45] I. Ganesh *et al.* 2012. Preparation and characterization of Fe-doped TiO_2 powders for solar light response and photocatalytic applications. *Processing and Application of Ceramics*. 6(1): 21–36. DOI: https://doi.org/10.1016/j.matchemphys.2012.04.062.

[46] H. Jensen *et al.* 2006. Determination of size distributions in nanosized powders by TEM, XRD, and SAXS. *Journal of Experimental Nanosciences.* 1(3): 355–373. DOI: https://doi.org/10.1080/17458080600752482.

[47] S. Salwa, Z. Harun, F. Hafeez, and K. Nazri. 2019. Enhancing the

performance of a hybrid porous polysulfone membrane impregnated with green Ag / AgO additives derived from the Parkia speciosa. *Vacuum*. 163: 301–311. DOI: https://doi.org/10.1016/j.vacuum.2019.02.034.

[48] K. M. Teck and S. A. Ibrahim. 2016. Effect of fe addition towards TiO_2 formation for photocatalytic activity. *ARPN Journal of Engineering and Applied Sciences*. 11(14): 8704–8709.

[49] S. R. Senthilkumar and T. Sivakumar. 2014. Green tea (Camellia Sinensis) mediated synthesis of zinc oxide (ZnO) nanoparticles and studies on their antimicrobial activities. *International Journal of Pharmacy and Pharmaceutical Sciences.* 6(6): 461-465.

[50] F. Zulkifli *et al.* 2017. The effect of concentration of Lawsonia inermis as a corrosion inhibitor for aluminum alloy in seawater. *Advances in Physical Chemistry.* 2017: 1-12. DOI: https://doi.org/10.1155/2017/8521623.

[51] R. Kumar, P. Sharma, A. Bamal, S. Negi, and S. Chaudhary. 2017. A safe , efficient and environment friendly biosynthesis of silver nanoparticles using Leucaena leucocephala seed extract and its antioxidant , antimicrobial , antifungal activities and potential in sensing. *Green Processing and Synthesis*. 6: 449–459. DOI: https://doi.org/10.1515/gps-2016-0146

[52] G. Rajakumar, A. A. Rahuman, B. Priyamvada, V. G. Khanna, D. K. Kumar, and P. J. Sujin. 2012. Eclipta prostrata leaf aqueous extract mediated synthesis of titanium dioxide nanoparticles," *Materials Letter.* 68: 115–117. DOI: https://doi.org/10.1016/j.matlet.2011.10.038

[53] G. Wang, L. Xu, J. Zhang, T. Yin, and D. Han. 2012. Enhanced photocatalytic activity of TiO_2 powders (P25) via calcination treatment. *International Journal of Photoenergy*. 2012: 1-9. DOI : https://doi.org/10.1155/2012/265760.

[54] S. Tabasideh, A. Maleki, B. Shahmoradi, E. Ghahremani, and G. McKay. 2017. Sonophotocatalytic degradation of diazinon in aqueous solution using iron-doped TiO_2 nanoparticles. *Separation and Purification Technology*. 189: 186–192. DOI: https://doi.org/10.1016/j.seppur.2017.07.065.

[55] W. Low and V. Boonamnuayvitay. 2013. Enhancing the photocatalytic activity of TiO_2 co-doping of graphene Fe^{3+} ions for formaldehyde removal. *Journal of Environmental Management*. 127: 142–149. DOI : https://doi.org/10.1016/j.jenvman.2013.04.029.

[56] T. Rasheed, M. Bilal, H. M. N. Iqbal, and C. Li. 2017. Green biosynthesis of silver nanoparticles using leaves extract of Artemisia vulgaris and their potential biomedical applications. *Colloids and Surfaces B: Biointerfaces*. 158(2017): 408–415. DOI: https://doi.org/10.1016/j.colsurfb.2017.07.020.

[57] C. Liao, Y. Li, and S. C. Tjong. 2020. Visible-light active titanium dioxide nanomaterials with bactericidal properties. *Nanomaterials*. 10(1): 1-56. DOI : https://doi.org/10.3390/nano10010124.

[58] S. Sagadevan. 2015. Investigation of the preparation and characterization of Fe-doped TiO_2. *Journal of Material Sciences and Engineering*. 4(3): 4–7. DOI: https://doi.org/10.4172/2169-0022.1000164

[59] F. Azeez *et al.* 2018. The effect of surface charge on photocatalytic degradation of methylene blue dye using chargeable titania nanoparticles. *Scientific Reports*. 8: 7104. DOI: https://doi.org/10.1038/s41598-018-25673-5.